Study of the composition, magnetic properties and stability of iron-nitride thin films deposited by reactive magnetron sputtering

D.H. Mosca, S.R. Teixeira, P.H. Dionisio, W.H. Schreiner and I.J.R. Baumvol

Instituto de Física, Universidade Federal do Rio Grande do Sul, P.O. Box 15051, 91500 Porto Alegre, RS, Brasil

Abstract   The deposition and thermal evolution of Iron-Nitride thin films produced by reactive spiittering has been investigated by X-ray diffraction, Mõssbauer conversion electron spectroscopy and magnetic measurements. The results show a similar composition of the films after thermal treatment at $500°C$, all being composed by α-Fe plus γ'-Fe_4N. The magnetic characteristics depend on the relative proportions of the end-products.

1. Introduction

The iron-nitrogen system has been studied for many decades due to its remarkable chemical and mechanical properties such as corrosion and wear resistance.

In the early 1970's[1] the magnetic properties of Fe-N thin films were reported and appeared to have both scientific and technological interest. Due to their good mechanical and magnetic properties, many authors suggested that the Fe-N compounds might have potential applications as magnetic recording heads and recording media[1-3].

The Fe-N binary system in bulk forms three compounds which are stable at room temperature. They are the Fe_8N, Fe_4N and Fe_2N [4]. The ferromagnetic iron nitride compounds Fe_xN with $2 < x < 8$ have saturation magnetization, even higher than pure iron[5].

The common deposition methods for iron-nitride thin film manufacture that appear in the literature are the ion beam assisted deposition (IBAD) and reactive sputtering deposition techniques, the last one receiving Iess attention.

This paper reports on the characterization, thermal stability and magnetic properties of iron nitride thin films deposited by dc reactive magnetron sputtering.

2. Experimental details

The iron-nitride films were deposited in a planar magnetron sputtering system. The base pressure of the chamber was 1×10^{-6} Torr. The total pressure during deposition was kept at 4×10^{-4} Torr by controlling the gas-flow rate. A mixture of pure Ar (99.97%) and pure N_2 (99.995%) was used as the sputtering gas. Three different compositions of Ar and N_2 were used to produce the films[6]. Silicon wafers (111) were used as substrates and the sample temperature did not exceed 60°C during deposition.

The film thicknesses and deposition rates were determined by 2-MeV a-particle Rutherford Backscattering Spectroscopy (RBS). The nitrogen concentration in the as deposited samples was determined by Auger electron spectroscopy (AES), as it is shown in table 1.

The characterization of the samples was made by Conversion Electron Mössbauer Spectrometry (CEMS) measurements in a backscattering geometry, using a ^{57}Co source in Rh matrix, and X-ray diffraction using the Cu K_α radiation.

The magnetic properties were studied using a vibrating sample magnetometer (VSM) in magnetic fields up to 5 kOe applied in the plane of the filrns.

In order to get some information about the stability of the phases formed during the deposition, the samples were submitted to sequential annealings in a high vacuum furnace at temperatures between 100 and 500°C during 60 min for each temperature[7].

Table 1 - Composition of Fe_xN as deposited thin films as measured by (AES).

Sample	PN_2	Composition
A	4×10^{-6} Torr	$Fe_{7.81}$ N
B	3×10^{-5} Torr	$Fe_{3.49}$ N
C	3×10^{-4} Torr	$Fe_{1.97}$ N

D . H. Mosca et al.

3. Results

Figure **1** shows the X-ray diffraction patterns for exarnple A $(P_{N_2} = 4 \times 10^{-6}$ Torr), (a) as deposited and (b) annealed at $500°C$ during 60 min. Fig. la should a broadened pattern around the (110) reflection of a-Fe, which can be identified as the (101) reflection of the ϵ-$(Fe_2N$-$Fe_3N)$ structure. Around $2\theta \approx 41°$ three appear's another broad diffraction line which cannot be univocally associated with a particular Fe-N compound. It can be associated with the (002) reflection of ϵ-$(Fe_2N$-$Fe_3N)$ and/or ϵ-(Fe_2N) or yet with the (111) reflection of γ'-Fe_4N. At $2\theta \approx 47^0$ a (200) reflection corresponding to γ'-Fe_4N can be also identified. In this same figure a small X-ray diffraction line assigned to the (102) reflection of ϵ-$(Fe_2N$-$Fe_3N)$ appears. After annealing at $500°C$ during 60 min, a great modification appears. The broadened structures transforms in well defined peaks correponding to the a-Fe and γ'-Fe_4N compounds. It is important to point out that during the annealing both phases a-Fe and γ'-Fe_4N grow and crystallize at expense of ϵ-$(Fe_2N$-$Fe_3N)$.

Figure **2a** shows the X-ray diffraction spectrum of sample B $(P_{N2} = 3 \times 10^{-5}$ Torr). The diffraction pattern shows a salient diffraction line identified as the (101) reflection of ϵ-Fe_3N. Besides that, we can identify two small peaks which are associated to the (002) ς-Fe_2N and (102) $Fe_2N(H)$, or (102) ϵ-$(Fe_2N$-$Fe_3N)$ compounds. After, at $500°C$ (fig. **2b**) the diffraction pattern modifies, showing only the γ'-Fe_4N compound. The a-Fe is absent indicating a different texture as compared with post-annealed sample A, fig. **1b**.

Fig. 3a shows the X-ray diffraction pattern corresponding to the as deposited sample C $(P_{N2} = 3 \times 10^{-4}$ Torr). The diffraction pattern shows a phase mixture of ς-Fe_2N and ϵ-$(Fe_2N$-$Fe_3N)$. After annealing at $500°C$ during 60 min the diffraction pattern in fig. **3b**, shows tht: (111) and (200) reflections, corresponding to the γ'-Fe_4N compound, like the other samples together with the reflections (200) and (110) of a-Fe. It is important to notice that the annealing again results in a different crystalline orientation of a-Fe as compared to the samples A and B.

150
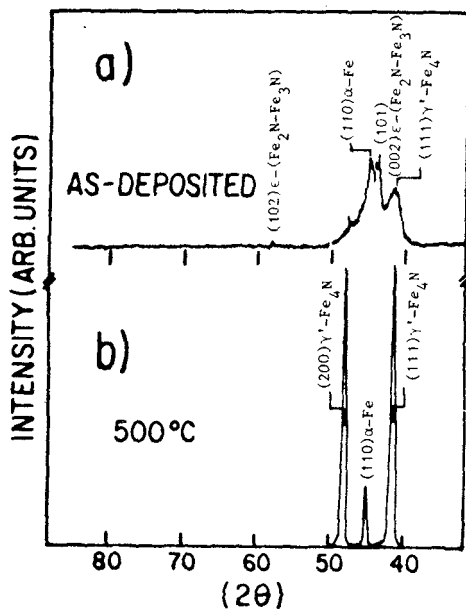
**Fig. 1 – X-ray diffractograms corresponding to sample A. a) as deposited and
b) annealed at 500°C during 60 min.**

Fig. 4a shows the CEMS spectrum of the as-deposited sample **A.** As can be seen, the spectrum is dominated by the sextet corresponding to the metallic α-Fe. This spectrum also shows another magnetic component which cannot be identified as a known Fe-N compound. The larger linewidth obtained in the fitting is apparently due to the spreading in the magnitude of the magnetic hyperfine fields due to a large disorder in the occupation of the nitrogen interstitial sites[8]. The CEMS spectrum obtained after the thermal treatment at 500°C is shown in fig. 4b. It shows a phase mixture of a-Fe together with γ'-Fe$_4$N. The relative spectral areas of α-Fe and γ'-Fe$_4$N are 60% and 40%, respectively (see Table **2)**. This thermal evolution is in perfect accordance with that depicted in the X-ray diffractogram of fig. 1.

Fig. **5** shows the CEMS spectra for sample B. The very complex spectrum shown in fig. 5a corresponds to the as deposited sample B. It can be interpreted
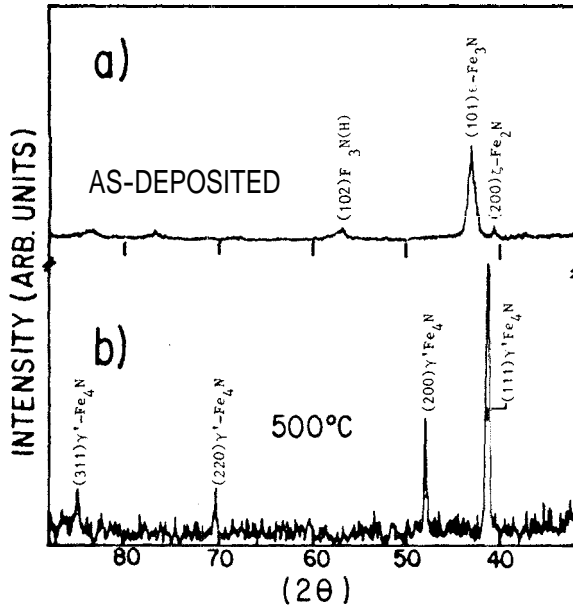
Fig. 2 – X-ray diffractograms of sample B. a) as deposited and b) after annealing
at 500°C during 60 min.

as the ferromagnetic Fe_xN ($x > 3$) phase coexisting with a paramagnetic $\varsigma\text{-}Fe_2N$ defficient in nitrogen[g]. The thermal treatment at 500°C, fig. 5b, shows a spectrum which can be ascribed to the $\gamma'\text{-}Fe_4N$ and a-Fe compounds. The relative areas for both compounds are **73** and 27% respectively (see the fitting parameters in Table **2**). If we compare the thermal evolution depicted in this figure with the one shown in fig. 2, we can see that only in fig. 5b we can identify the presence of $\alpha\text{-}Fe$. This apparent discrepancy can be iinderstood on the basis of crystalline orientation of the a-Fe which prevents it from being detected by X-ray diffraction.

Sample C display the CEMS spectra shown in fig. 6. In fig. 6a, the spectrum for the as deposited sample was taken in a reduced velocity scale. We identify a broadened doublet which is attributable to the y—Austenite. The $\varsigma\text{-}Fe_2N$ is incomplete. After the thermal treatment at 500°C, the spectrum shown in fig. 6b, displays again $\alpha\text{-}Fe$ together with $\gamma'\text{-}Fe_4N$. A small difference, liowever, exists when we compare this spectrum with the spectra showed in fig. 4a and fig. 5b.
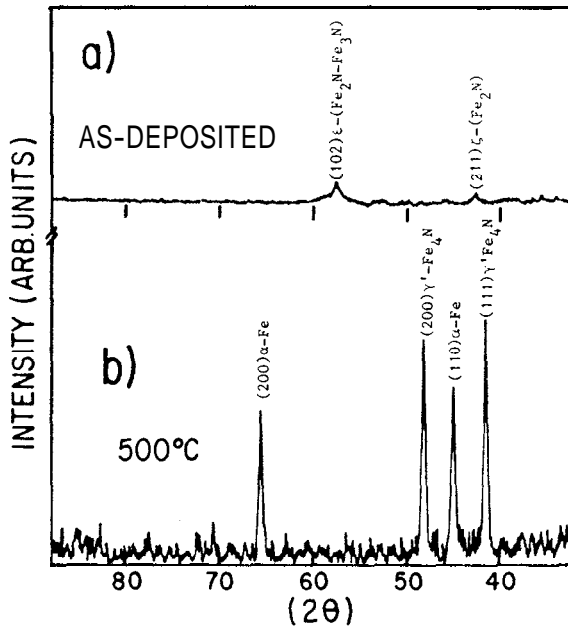
Fig. **3** – X-ray diffractograms of sample C. a) as deposited and b) after annealing at 500°C during 60 min.

The central part of the spectrum shows a quadrupole doublet, which corresponds to $\epsilon\text{-Fe}_2\text{N}$ within an overwhelming ferromagnetic matrix. The relative areas corresponding to a-Fe and $\gamma'\text{-Fe}_4\text{N}$ are **43** and **52%**, respectively (see Table **2**).

Fig. 7 shows the in-plane hysteresis loops measured by VSM at room temperature. According to figs. 7a and 7b, in as deposited condition, the saturation magnetizations of samples A and B are similar, being smaller than the saturation magnetization of the pure iron film. This smaller magnetization of samples A and B is due in part to the coexistence of paramagnetic phases with ferromagnetic phase, as can be seen in the X-ray and CEMS analyses showed in fig. 1a, 2a, 4a and 5a.

The coercitivity of sample A and B are **33** and 36 Oe, respectively. These coercitivities are smaller than the coercitivity of a pure iron film.

Figs. 7c, 7d and 7e show the in-plane hysteresis loops for samples A, B and C after annealing at 500°C during 60 min, respectively. The magnetization axis
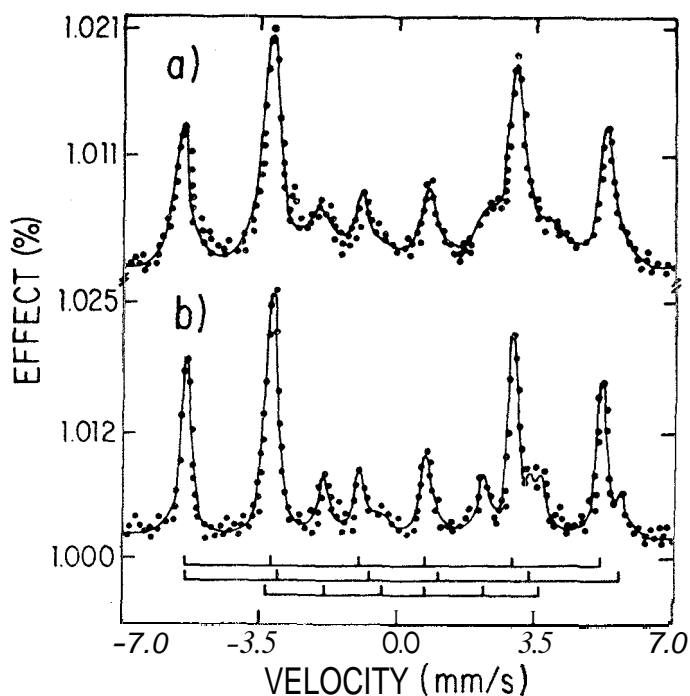
Fig. 4 – CEMS spectra of sample A. a) as-deposited and b) after annealing at 500°C during 60 min.

is in arbitrary units. Depending on the original nitrogen content in the sputtering chamber during deposition, two different trends are observed after annealing. First, the coercitivity increases with the increase of N_2 pressure in the chamber: 51 Oe for sample A, 61 Oe for sample B and 150 Oe for sample C. Second, the squareness of the hysteresis loops is enhanced in the case of sample B and C post-annealed. Fig. 7e displays a squareness factor of 0.86, which is very close to the values obtained for acircular Fe_4N particulates[10].

4. Conclusions

As it was expected, the nitrogen content in the thin Fe_xN films increases with the N_2 partial pressure in the sputtering plasma, resulting in a homogeneous concentration of nitrogen as a function of depth.

Table 2 - Mõssbauer fitting parameters of the as deposited and annealed samples together with the identification of phases and their relative spectral areas (the Isomer shifts are quoted with respect to Fe in Rh).

Sample	T(°C)	H(kOe)	ΔE_Q(mm.s)$^{-1}$	γ(mm.s)$^{-1}$	Γ	%	Ident
A	R.T.	330	0	-0.10	0.38	59	a-Fe
		355.8	0.004	0.008	0.53	5	?
		226	0.10	0.21	0.87	36	?
	500	330	0	-0.11	0.25	41	α-Fe
		347	Q004	0.008	0.48	23	$\gamma'Fe_4N$
		226	0.105	0.22	0.67	36	$\gamma'Fe_4N$
B	R.T.	265	0	0.26	0.47	11	$Fe_{2+z}N$
		207	0	0.23	0.48	31	$Fe_{2+z}N$
		179	0	0.20	0.42	4	$Fe_{2+z}N$
		78	0	0.19	0.55	38	$Fe_{2+z}N$
		-	0.87	0.26	0.58	1	Fe_2N
		-	0.47	0.30	0.35	15	Fe_2N
	500	330	0	-0.09	0.29	27	α-Fe
		345	0.05	0.14	0.43	73	$\gamma'Fe_4N$
		217	0.02	0.29	0.37	73	$\gamma'Fe_4N$
C	R.T.		0.41	0.26	0.37	100	Fe_2N
	500	330	0	-0.10	0.24	43	α-Fe
		343	-0.017	0.15	0.27	52	$\gamma'Fe_4N$
		217	0.03	0.18	0.36	52	$\gamma'Fe_4N$
		-	0.43	0.26	0.65	5	Fe_2N

Due to low deposition temperature, common in the magnetron sputtering method, the high magnetization nitrides as Fe_8N and Fe_4N are absent in the as deposited samples. High temperature processes, as diode sputtering, can lead to the formation of Fe_8N and Fe_4N [11-14].

The small saturation magnetization (as compared to pure iron films is due to presence of the paramagnetic ϵ-Fe_2N phase and the moderate coercitivities with a moderate in plane magnetic anisotropy. This is a characteristic of the low temperature deposition'methòds since the nitrogen-rich nitrides nucleates around
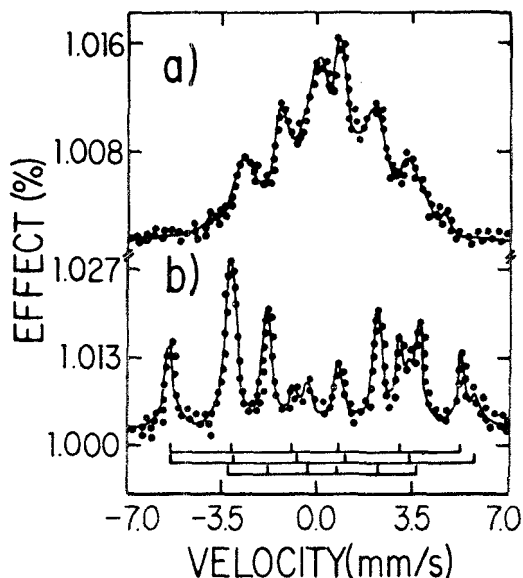
Fig. 5 – CEMS spectra of sample B. a) as-deposited and b) after annealing at 500°C during 60 min.

room temperatures, while the Fe-rich nitrides are prevented from nucleating at these temperatures[3,10]. The phase inhomogeneity can also be attributable to the low temperature during deposition, even in the case of sample X where the Fe_2N compound appears together with the randomic occupation of interstitial sites by nitrogen atoms, as was revealed by CEMS and X-ray analyses.

The films rearrange under thermal treatment at 200-300°C. The highly disordered phases transform as interstitials and defects migrate. At temperatures above 400°C some nitrides decompose and the nitrogen seems to leave the samples, resulting in Fe-richer phases as $\gamma'-Fe_4N$ plus a-Fe.

It is important to point out that sample B has a smaller a-iron content than the other samples after annealing at 500°C. We note that the hexagonal Fe_3N phase is present only in this sample, suggesting that some mechanism involving the decomposition of this phase can prevent the full a-Fe precipitation.
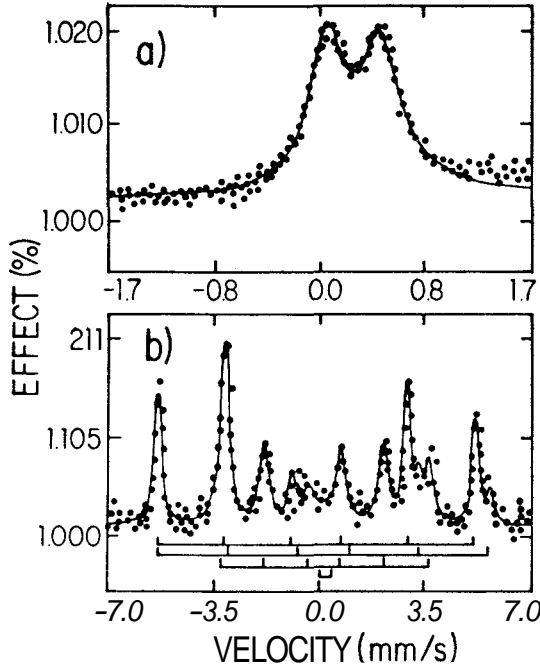
Fig. 6 – CEMS spectra of sample C. a) as-deposited and b) after annealing at 500°C duririg 60 min.

From a magnetic point of view, the measurements show that the samples are more interesting for practical purposes after annealed at 500°C than in as deposited condition.

The ferromagnetic behaviour of all samples is apparent after thermal treatment. Specially sample C is magnetically interesting. It has high magnetization due to the pure α-Fe and γ'-Fe$_4$N phases, which have similar magnetizations, apreciable squareness and remanence and a still moderate in plane coercive field. The higher coercitivity, of course, can arise out of magnetic interplay of γ'-Fe$_4$N and a-Fe, together with the paramagnetic ϵ-Fe$_2$N compound, still present after annealing, or a different orientation of a-Fe precipitates as can be seen in the X-ray diffractogram of fig. 3.
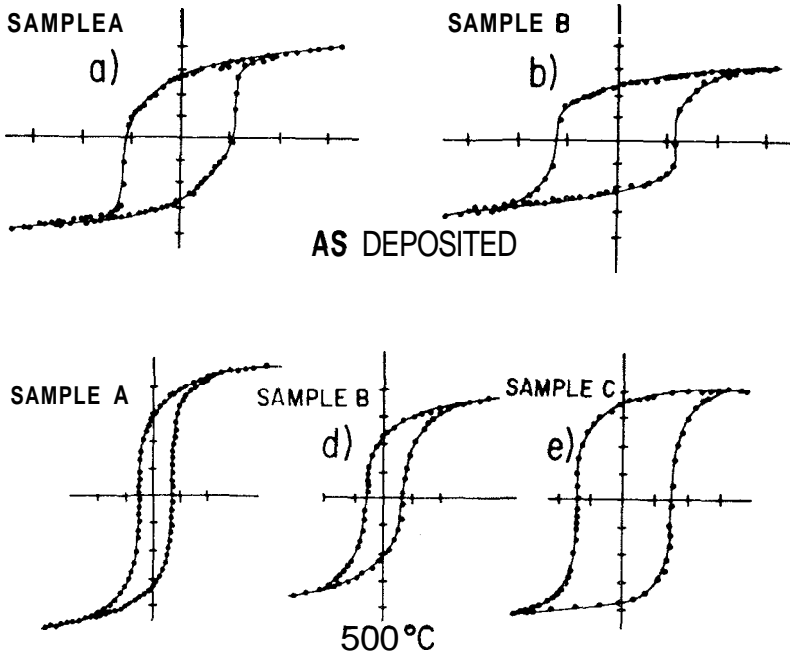
Fig. 7 – **Hysteresis loops of samples A and B in the deposited conditions, part a) and b) respectively. Part c, d and e correspond to the hysteresis loops for samples A, B and C after thermal treatment.**

On the other hand, it can be pointed out that certain relative proportions of α-Fe and γ'-Fe$_4$N can produce magnetic quantities such as squareness and coercitivity, however the exact mechanisms responsíble for this behaviour are not clear at present.

References

1. T. K. Kim and Takahashi, Appl. Phys. Lett., 20, **492 (1972).**

2. **K.** Tagawa, E. Kita and A. Tasaki, Jap. **J.** Appl. Phys., 21, **1596 (1982).**

3. N. Saegusa, **T.** Tsukagoshi, E. Kita and **A.** Tasaki., IEEE Trans. Magn. Mag., 19, **1629 (1983).**

4. **B.** Kubaschewski, *Iron-Binary Phase Diagrams* (Springer, New York, **1982**) p. **67**.

5. N. Terada, Y. Hoshi, M. Naoe and S. Yamanaka, IEEE Trans. Magn. Mag, 20, **1451 (1984).**

6. D. H. Mosca, P. H. Dionisio, W. H. Schreiner and I. J. R. Baumvol, J. Appl. Phys. 67, **7514 (1990).**

7. D. H. Mosca, S. R. Teixeira, P. H. Dionisio, I. J. R. Baumvol and W. H. Schreiner. To appear in J. Appl. Phys.

8. N. De Cristoforo and R. Karplow, Mettal. Trans. **A8, 425 (1977).**

9. M. Mekata, **H.** Yoshimura, and H. Takoki, J. Phys. Soc. Jap., 33, **62 (1972).**

10. K. Umeda, E. Kita and **A. Tasaki,** IEEE Trans. Magn. Mag., 22, **591 (1986).**

11. **H.** De Rugy, J. P. Langeron, S. Bouquet, L. Minel, G. I. Grigorov and I. N. Martev, Thin Sol. Films, 161, **L69 (1988).**

12. N. Nagakubo, T. Yamamoto and M. Naoe, J. Appl. Phys., 63, **4309 (1988).**

13. **J.** Lo, **L.** Franco, T. C. Huang, T. W. Wu, D. Miller and R. Campbell, IEEE Trans. Magn. Mag., 24, **3081 (1988).**

14. M. Naoe, M. Nagakubo and I. Iamamoto, J. Appl. Phys., 64, **5449 (1988).**

Resumo

A deposição e a evolução térmica de filmes de Nitreto de Ferro por erosão catódica reativa foi investigada por Difração de Raios-X, Espectroscopia Mössbauer de elétrons de conversão e medidas magnéticas. Os resultados mostram uma composição semelhante para filmes após tratamento térmico a $500°C$, sendo formados pelas fases a-Fe e γ'-Fe_4N. As características magnéticas dependem da proporção relativa entre os produtos finais.